Chemical Physics Letters 581 (2013) 64–69

Contents lists available at SciVerse ScienceDirect

Chemical Physics Letters

journal homepage: www.elsevier.com/locate/cplett

Supercapacitance of chemically converted graphene with composite pores

Ming Zhou [a], Tian Tian [a], Xuanfu Li [a,b], Xudong Sun [a], Juan Zhang [a,b], Youhu Chen [a], Ping Cui [a], Jie Tang [c], Lu-Chang Qin [a,d,*]

[a] Division of Functional Materials and Nano Devices, Ningbo Institute of Materials Technology and Engineering, Chinese Academy of Sciences, Ningbo 315201, China
[b] School of Chemistry and Chemical Engineering, Ningbo University, Ningbo 315201, China
[c] National Institute for Materials Science, Tsukuba 305-0047, Japan
[d] Department of Physics and Astronomy, University of North Carolina at Chapel Hill, Chapel Hill, NC 27599-3255, USA

ARTICLE INFO

Article history:
Received 23 May 2013
In final form 28 June 2013
Available online 5 July 2013

ABSTRACT

We report the synthesis and characterization of chemically converted graphene (CCG) with composite pores that has exhibited high specific capacitance (up to 350 F g^{-1}). The porous CCG was obtained by photocatalytic reaction aided by ZnO quantum dots and it has both macropores (>50 nm) and meso/micro-pores (<10 nm). The introduction of macropores allowed penetration of electrolyte into the inter-layer space of CCG while the meso/micro-pores increased the adsorption of charges. The supercapacitor made from such porous CCG also exhibited excellent rate performance and cyclic stability.

1. Introduction

With the fast development of portable electronics and hybrid electrical vehicles, there has been an ever increasing demand for energy storage devices. Supercapacitors, which store and release energy by nanoscopic charge seperation at the electrode–electrolyte interface, have attracted great attention due to their high charging/discharging rate, long cycle life, and superior stability [1,2]. On the other hand, although they are able to provide high-power energy, supercapacitors are limited in the amount of energy stored measured in gravimetric and/or volumetric energy densities. The amount of energy stored in a supercapacitor is usually evaluated by its specific capacitance and it is largely determined by the specific surface area of the electrode material. Graphene, a two-dimensional single-atom thick nanomaterial of carbon, possesses a theoretical specific surface area of 2630 m^2 g^{-1}, which is comparable to that of best activated carbon and is a promising candidate electrode material for supercapacitors [3–6]. The intrinsic capacitance of graphene is 21 μF cm^{-2}, which is the highest among all carbon forms [7]. Furthermore, modified graphene with meso/micro-pores can increase further the specific capacitance of graphene. This strategy is based on the fact that the adsorption of charges by edge atoms is much larger than that by the interior atoms [8]. The currently available methods for producing meso/micro-pores in graphene include KOH activation [9], MnO_4^- oxidation [10], and chemical vapor deposition (CVD) [11]. All these methods have been proved efficient for producing graphene with high specific surface area. However, the specific capacitance of graphene obtained experimentally is still far below its theoretical value of 550 F g^{-1}. A major problem is that the restacking of graphene during reduction and drying leaves much of the inter-layer space not accessible to the electrolyte and hence does not contribute to the electrochemical double-layer capacitance. Modification of graphene to produce either curved or highly corrugated morphology has been attempted to prevent graphene from re-stacking [12,13]. Another effective technique has been to insert nano-sized spacers, such as carbon nanotubes (CNTs) and metal oxide nanoparticles into graphene [14,15].

In this work, we describe a porous chemically converted graphene (CCG) containing both meso/micro-pores (<10 nm) and macropores (>50 nm) (termed composite pores thereafter). Using the porous CCG, we demonstrate that, even though the specific surface area is rather low, the porous CCG electrodes exhibit excellent electrochemical capacitance (up to 350 F g^{-1}), rate performance, and cyclic stability. The electrochemical process and material structure are also characterized to understand the high specific capacitance and excellent device performance of the constructed graphene supercapacitor.

2. Experimental

2.1. Preparation of CCG with composite pores

Graphene oxide (GO) was prepared from natural graphite by a modified Hummers–Offeman method [16]. ZnO quantum dots

* Corresponding author at: Department of Physics and Astronomy, University of North Carolina at Chapel Hill, Chapel Hill, NC 27599-3255, USA. Fax: +1 9199620480.
E-mail address: lcqin@email.unc.edu (L.-C. Qin).

0009-2614/$ - see front matter © 2013 Elsevier B.V. All rights reserved.
http://dx.doi.org/10.1016/j.cplett.2013.06.063

(QDs) were synthesized by alcoholysis using zinc acetate as precursor [17]. In detail, GO and ZnO QDs were first dispersed ultrasonically in deionized water. They were then mixed together and heated to 90 °C in an oil bath to have ZnO QDs adsorbed onto the GO surface. After it was cooled down to room temperature, the suspension was placed under a UV lamp for irradiation for 12 h while being stirred. Then, concentrated hydrochloride acid was added to the suspension to remove the ZnO QDs. The GO suspension was then vacuum filtered using a Nylon membrane of 0.22 μm in pore size. The resultant residues were washed three times with deionized water and then transferred to 200 ml deionized water containing $NH_3 \bullet H_2O$. The GO became well dispersed in water after sonication. The resultant GO dispersion was then transferred to an autoclave and heated to 180 °C for hydrothermal reduction. Porous CCG was obtained finally after the dispersion was freeze dried.

2.2. Fabrication of supercapacitor electrodes

The supercapacitor test cells were assembled in the two-electrode configuration using 6 M KOH electrolyte. Identical electrodes were made of CCG mixed with 10 wt% polytetrafluoroethylene (PTFE). The electrodes were vacuum dried at 120 °C for 18 h and then pressed onto current collectors made of nickel foam plates at pressure of 20 MPa. Two glass fiber films were used as the separator to obtain a CR2016 coin cell for device evaluation.

2.3. Electrochemical measurements

The electrochemical properties and capacitance measurements were conducted in a two-electrode configuration by cyclic voltammetry (CV), galvanostatic charge–discharge, and electrochemical impedance spectroscopy (EIS) using a Zennium electrochemical workstation. The CV response of the electrodes was measured at different scan rates varying from 10 to 200 mV s^{-1} at potentials between −1 and 0 V. Galvanostatic charge–discharge measurements were performed at different current densities varying from 0.5 to 4 A g^{-1}. EIS measurements were carried out at open circuit voltage with sinusoidal signal of 5 mV over the frequency range from 100 kHz to 10 mHz.

2.4. Structural characterization

Atomic force microscopy (AFM) measurements were performed using Veeco Dimension 3100 V scanning probe microscope at ambient conditions. GO and CCG samples for AFM measurement were prepared by dip-coating. In brief, a mica plate was immersed in CCG (or GO) dispersion (0.001 mg mL^{-1}, in N-methyl-2-pyridine) for 5 min to adsorb a thin layer of graphene flakes and then was immersed in deionized water for another 5 min to remove the unadsorbed CCG. Transmission electron microscopy (TEM) images were taken with Tecnai F20 operated at 200 kV. N_2 absorption/desorption tests were conducted using Micromeritics ASAP 2020 M. X-ray photoelectron spectroscopy (XPS) measurements were carried out using a Shimadzu Axis Utltradld spectrometer with a monochromated Al Kα radiation ($h\nu$ = 1486.6 eV). All XPS spectra were corrected using the C 1s line at 284.6 eV. Curve fitting and background substraction were conducted using Casa XPS software (Version 2.2.7.3).

3. Results and discussion

3.1. Preparation of CCG with composite pores

The process for production of porous CCG consists of three steps, as shown schematically in Figure 1: (a) incorporation of ZnO QDs onto the GO surface; (b) UV irradiation induced photochemical reactions to produce composite pores in GO; and (c) acid treatment to remove ZnO QDs and hydrothermal reduction of GO to obtain CCG. The incorporation of ZnO QDs onto the GO surface was achieved by heating aqueous ZnO/GO dispersion in an oil bath. The large affinity of oxygen containing functional groups to Zn would lead to adsorption of ZnO QDs on the GO surface [18]. When the ZnO/GO mixed suspension was irradiated by a UV light, the following photochemical reactions took place to result in the formation of macro-pores on the GO surface [19]:

$$C-O-C+H_2O+2h^+ \rightarrow C(\text{defect})+CO_2+2H^+ \quad (1)$$

$$C-O-C+2h^++2e^- \rightarrow C-C(\text{defect})+H_2O \quad (2)$$

$$2H_2O(\text{or } H^+)+2e^- \rightarrow H_2+2OH^- \quad (3)$$

$$C(\text{defect})+2H_2O+4h^+ \rightarrow CO_2+4H^+. \quad (4)$$

The π-conjugated sp^2 semiconducting domains in GO were responsible for these reactions. As some of them had band gaps with energy matching to that of the UV light, holes and electrons were produced when the sample was irradiated by UV light. The reactions of holes and electrons with oxygenated sp^3 domains in GO and subsequent oxidation of carbon atoms to form carbon dioxide would produce macropores on the GO surface. On the other hand, since it is a semiconductor, ZnO could also serve as photocatalyst to produce holes and electrons in UV light. However, as these holes and electrons were more preferred to react with neighboring carbon atoms, photo-reactions took place only at the ZnO-GO interfaces and hence only meso/micro-pores of a few nanometers in size were produced. After the obtained ZnO/GO composite was subsequently treated by hydrochloric acid to remove the ZnO QDs, a dispersion containing GO with composite pores was obtained. Hydrothermal treatment of the GO dispersion was finally used to reduce GO to obtain CCG [20].

3.2. Structural characterization

The TEM images of GO, ZnO QDs, ZnO/GO composite, and CCG with composite pores are shown in Figure 2. It can be seen from Figure 2a that the GO is ultra-thin with wrinkled morphology and no pores were present in the GO structure. The ZnO QDs, as shown in Figure 2b, are of size ranging from 3 to 6 nm and they are well dispersed. As revealed in the TEM image of the ZnO–GO mixture given in Figure 2c, the ZnO QDs were deposited and dispersed well on the GO surface. Figure 2d shows a TEM image of both meso/micro-pores (<10 nm) and macropores (>50 nm). While TEM observations are helpful to reveal porous structures, it is still a formidable task to analyze the pores quantitatively from TEM images alone.

Figure 3a shows the AFM image of a typical GO flake. No pore was observed on the GO surface. Thickness of the GO is about 0.9 nm on average, calculated from the height difference between the surface of GO and that of the substrate measured along the line indicated in the figure. This thickness is consistent with single layer GO [21]. By sampling randomly seventy GO sheets we constructed a histogram of the layer numbers of GO as shown in Figure 3c. It shows that more than 90% of the GO is of monolayer. A typical AFM image of CCG is shown in Figure 3b. The CCG has many pores. Thickness of the majority of CCG samples is about 1.0 nm. It corresponds to two- or three-layer graphene as the interlayer spacing of CCG will decrease after reduction due to the removal of oxygen functional groups. By carefully examining the height profiles of the CCG as indicated in the inset of Figure 3a and b, we also observed that the depth of the pores is

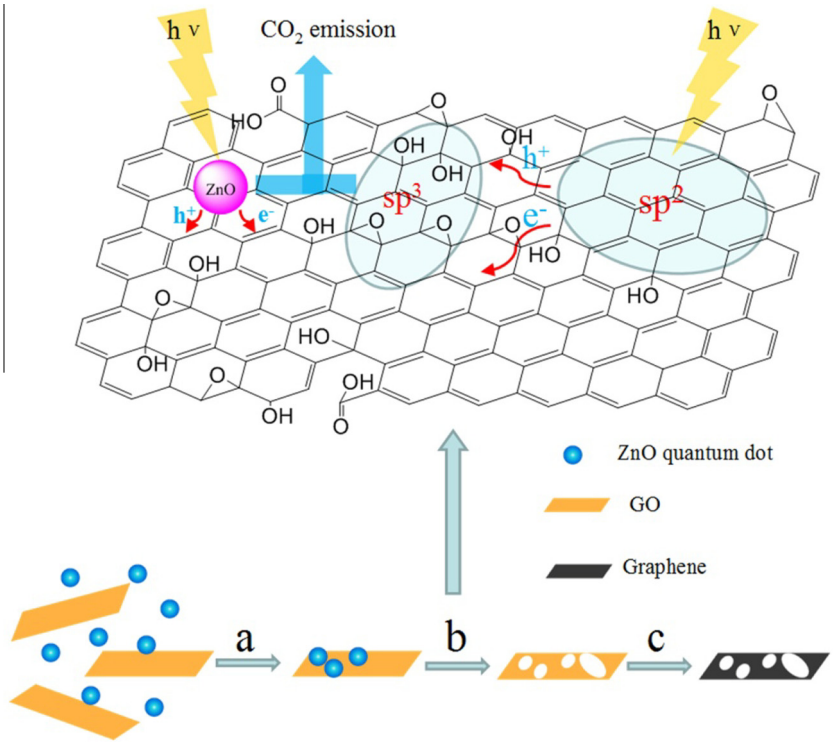

Figure 1. Illustration of production procedures of porous CCG and formation of pores with various sizes.

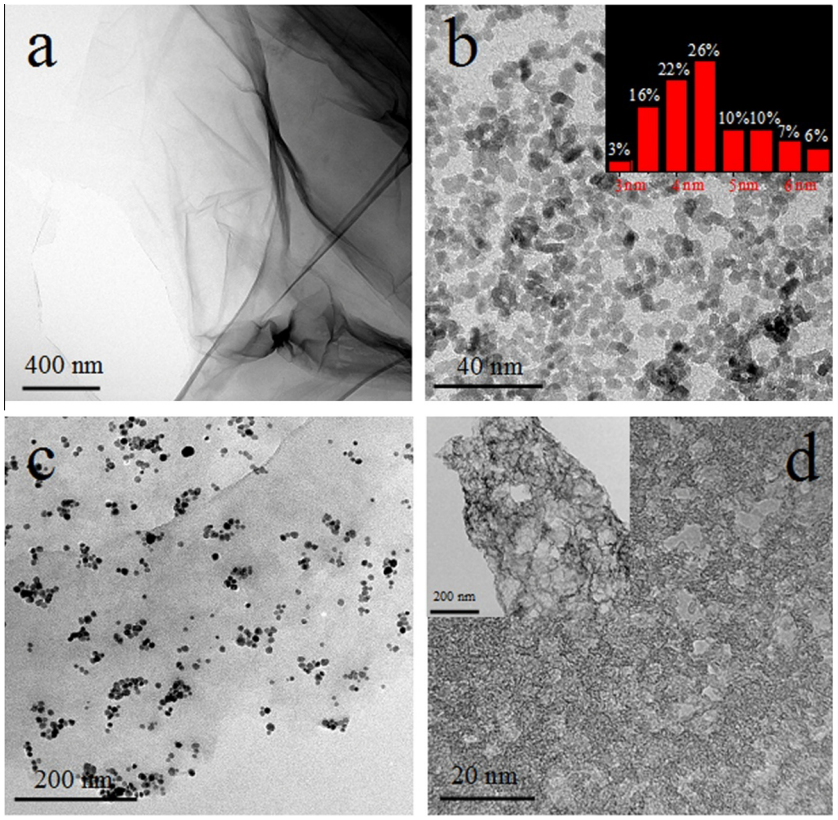

Figure 2. TEM image of (a) GO, (b) ZnO QDs (inset shows their size distribution), (c) ZnO QDs dispersed on the GO surface, and (d) CCG with composite pores. The inset in (d) is a low-magnification TEM image showing the macropores.

one half of the thickness of the CCG. Figure 3d is a histogram of layer numbers of CCG showing that more than 85% of the graphene is of bilayer structure.

The C:O mass ratio in the porous CCG is about 8.2, which was measured from XPS and it is larger than most of the C:O ratio obtained by other reducing methods [13]. No signal corresponding to

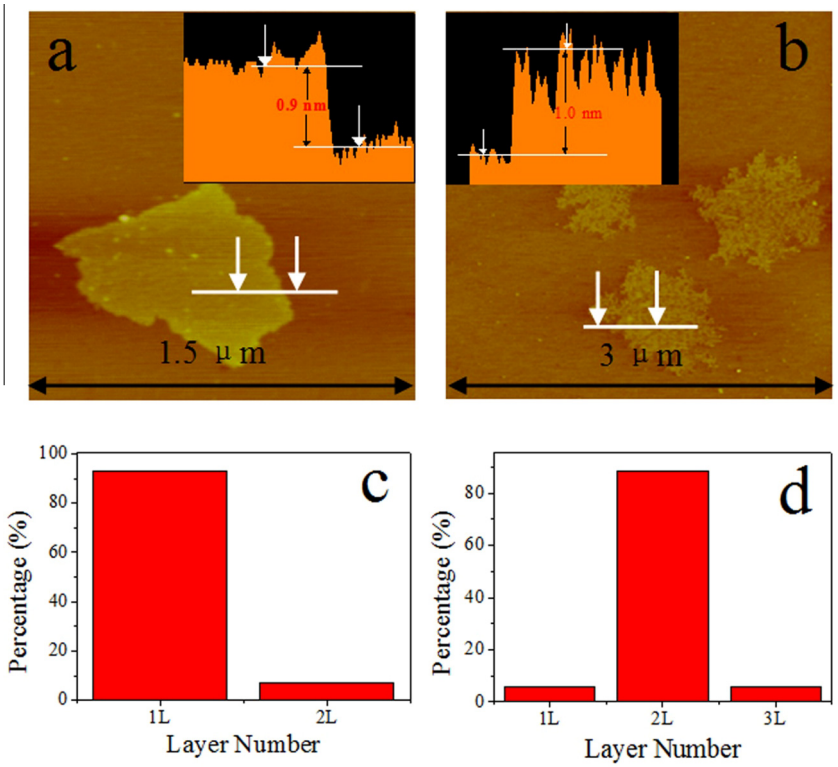

Figure 3. AFM image of (a) GO and (b) CCG with composite pores and their respective height profile (inset) measured along the indicated line. (c,d) Histogram of layer numbers obtained from randomly selected seventy samples of GO and CCG with composite pores, respectively.

Zn was observed in XPS, indicating that the ZnO QDs had been removed by the acid treatment.

N_2 adsorption/desorption experiment was performed on the porous CCG for analysis of the pore structure and size distribution. Figure 4a shows the isotherm which reveals the details of the low-pressure region where micro-pore filling occurs, as well as the linear plot in the relative pressure P/P_0 in the range of 0.3–0.6 that reveals pore condensation and type H2 hysteresis that is associated with mesoporosity [22]. It is worth noting that there is no hysteresis formed between the adsorption and desorption isotherms over the whole P/P_0 range. This may be because many slit pores were produced around the graphene boundaries due to the aggregation of graphene sheets. The Brunauer–Emmett–Teller (BET) surface area of our porous CCG is 392 $m^2\ g^{-1}$ calculated by the multipoint BET method in the linear relative pressure range of 0.1–0.3. This value of specific surface area is much lower than what is expected for double-layer graphene (1300 $m^2\ g^{-1}$), suggesting that the CCG must have further restacked after freeze drying. Figure 4b displays the cumulative pore volume vs. pore size obtained from N_2 desorption isotherms by applying the Barrett–Joyner–Halenda method. It can be seen that the size of the meso/micro-pores centers at 3.5 nm with its majority below 5 nm. This result is in agreement with TEM observations.

3.3. Electrochemical characterization

Experimental measurement of the capacitance of supercapacitors depends strongly on the cell configuration and it is always higher when using a three-electrode system [23]. A coin cell (two-electrode system) was therefore used in this work to obtain accurate measurement of the material performance of the supercapacitor electrode [24]. For comparison, non-porous CCG and macroporous CCG were also prepared and assembled into coin cells. Non-porous CCG was produced by hydrothermal reduction of GO (ZnO QDs were first dispersed onto GO and was subsequently treated with hydrochloric acid to remove these particles) without UV light treatment. Macroporous CCG was produced using the same method as that for the production of CCG with composite pores

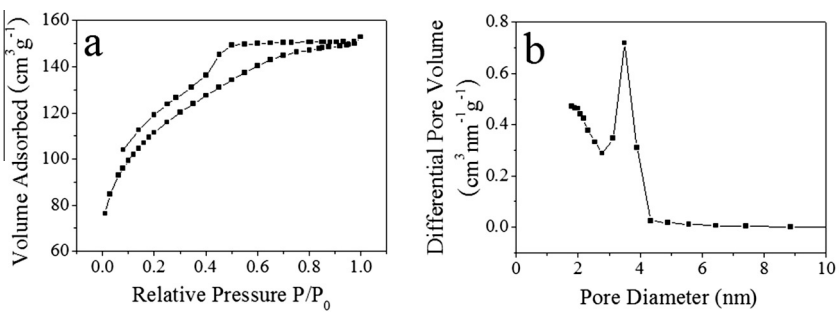

Figure 4. (a) N_2 adsorption/desorption isotherm of porous CCG and (b) its pore size distribution obtained using the Barrett–Joyner–Halenda method.

except that no ZnO QDs were added to the aqueous GO dispersion. The production of macro-porous and non-porous CCG was confirmed by TEM observations of the respective samples similar to those shown in Figure 2.

To prepare supercapacitor electrodes, the above mentioned three types of CCG were all mixed with 10 wt% PTFE and pressed onto nickel foam plates as current collectors. After vaccum dried at 120 °C for 18 h, the active material of each type was weighed from the weight difference of current collectors before and after loading. The thickness of electrode was measured from cross-sectional SEM images. Table 1 lists the measured parameters.

Figure 5a shows the CV curves of the three different electrodes at scan rate of 10 mV s^{-1} in 6 M KOH electrolyte. The rectangular CV loop indicates that there is little faradic discharge in the supercapacitor. It is worth noting that the CV loops for the CCG with composite pores and the macroporous CCG are more rectangular than that for the non-porous CCG, indicating better charge propagation in the porous CCG electrodes. Figure 5b shows the galvanostatic charge/discharge curves of the three electrodes at constant current density of 1 A g^{-1}. All the curves are symmetrical, indicating excellent electrochemical reversibility. However, the voltage drop (IR drop) for non-porous CCG is larger than that for porous CCG, suggesting that the non-porous CCG electrode has a higher internal resistance. This result is in agreement with that obtained by the above analysis of the CV curves. The specific capacitance was calculated from the galvanostatic charge/discharge curves by

$$C = 4\frac{I_{cons}}{m\,dv/dt} \tag{5}$$

where I_{cons} is the constant current, m is the total mass of both electrodes, and dV/dt is calculated from the slope obtained by fitting a straight line to the discharge curve over the range of V_{max} (voltage at the beginning of discharge) to $V_{max}/2$. The specific capacitance of the three different CCG electrodes at current density ranging from 0.5 to 4 A g^{-1} is shown in Figure 5c. With increasing current density, the specific capacitance of CCG with composite pores decreased only slightly, from 218 F g^{-1} to 205 F g^{-1}. This result demonstrates the outstanding rate performance of the electrode made of CCG with composite pores at high rates of charging/discharging.

The specific capacitance of 218 F g^{-1} measured at 0.5 A g^{-1} is comparable to that of hydrazine reduced graphene (~190 F g^{-1}) [25], microwave-exfoliated and reduced graphene (174–182 F g^{-1}) [26], and CVD grown porous graphene (~245 F g^{-1}) [11] measured under the same conditions.

The cyclic stability is also important for evaluating the performance of supercapacitors. We performed CV tests for 2000 cycles at 200 mV s^{-1} from 0 to −1 V and the results are given in Figure 5d, showing that the CCG with composite pores retained 95% specific capacitance after 2000 cycles.

The specific capacitance of the CCG electrode could also be calculated from the CV loop by

$$C = 4\int_{-1}^{0} I_m dV/(\upsilon V_0) \tag{6}$$

where I_m is the response current density (A g^{-1}), V is the potential with maximum V_0 = 1 volt and υ is the potential scan rate (mV s^{-1}). The highest specific capacitance of 350 F g^{-1} was obtained for electrode made of CCG with composite pores, which is markedly larger than those of reported values for porous graphene electrode even with much larger specific surface area, such as MnO_2 etched porous graphene (241 F g^{-1}, 1374 m^2 g^{-1}) [10] and CVD grown porous graphene (255 F g^{-1}, 1654 m^2 g^{-1}) [11] measured under the same

Table 1
Thickness and mass loading of sample electrode.

Electrode	Nonporous CCG	Macroporous CCG	CCG with composite pores
Thickness (μm)	110	80	85
Mass loading (mg)	5.0	3.7	3.7

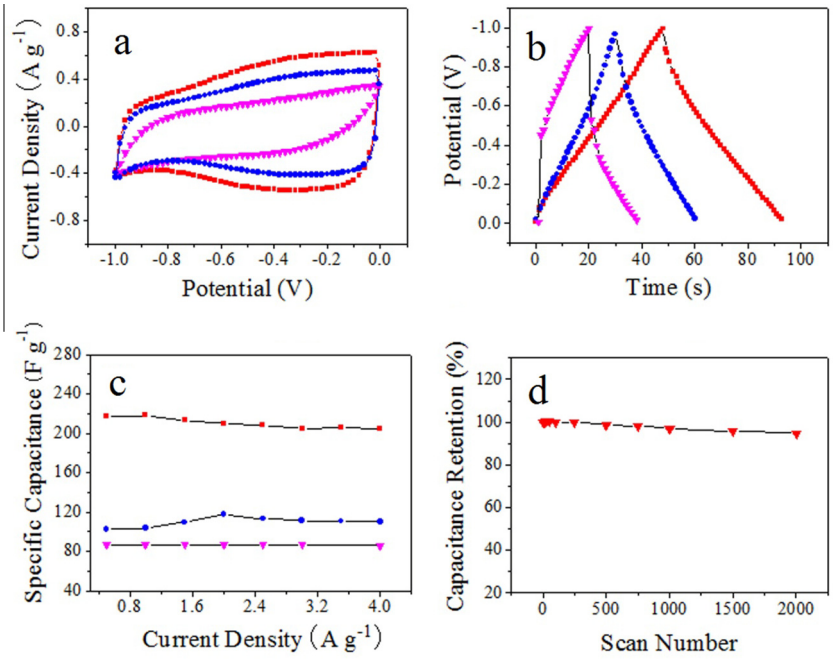

Figure 5. Electrochemical characterization of supercapacitors with electrodes made of non-porous CCG (triangle/pink), macroporous CCG (solid circle/blue) and CCG with composite pores (square/red). (a) CV curves in 6 M KOH electrolyte at scan rate of 10 mV s^{-1}. (b) Galvanostatic charging/discharging curves in 6 M KOH electrolyte at the same current density of 1 A g^{-1}. (c) Specific capacitance obtained from galvanostatic charging/discharging curves at different current densities. (d) Cyclic performance supercapacitor made of CCG with composite pores up to 2000 cycles at scan rate 200 mV s^{-1}. (For interpretation of the references to colour in this figure legend, the reader is referred to the web version of this article.)

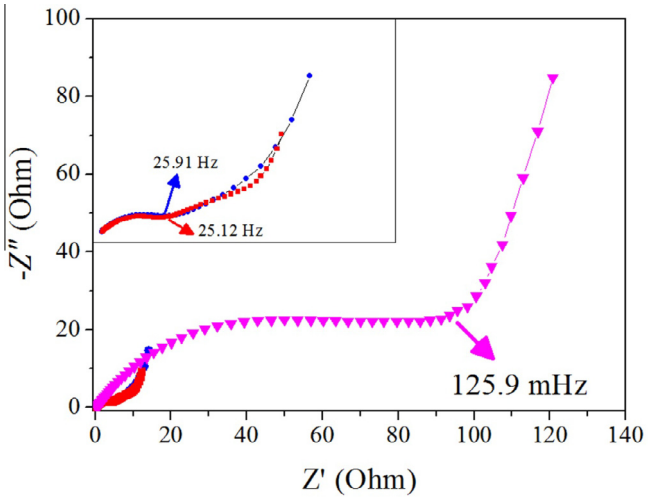

Figure 6. Nyquist plot of EIS data of non-porous CCG (triangle/pink), macroporous CCG (solid circle/blue) and CCG with composite pores (square/red). Inset shows magnified portion for macroporous CCG and CCG with composite pores. Arrow indicates the starting frequency of the Warburg curve. (For interpretation of the references to colour in this figure legend, the reader is referred to the web version of this article.)

conditions. However, it should be noted that the value of specific capacitance calculated from CV loops is usually much larger than that obtained from galvanostatic charging/discharging curves. It is because the supercapacitor can be fully charged, when the scan rate $v = dV/dt$ is held at constant and low values, as can be observed at the high voltage values in the CV curve. We examined four more devices and the difference between the highest and lowest specific capacitance is smaller than 4%, indicating excellent reproducibility of such high capacitance. Moreover, the specific capacitance at scan rates ranging from 10 to 200 mV s^{-1} for CCG with composite pores is always larger than that for both the macroporous and non-porous CCG, indicating that the introduction of both macropores and meso/micro-pores improved the electrochemical capacitance of the CCG electrodes. It was also noticed that the specific capacitance of all electrodes decreased with scan rates. This phenomenon is attributed to the fact that the measured apparent capacitance is limited by ion diffusion and adsorption inside the smaller pores at high scan rates.

To further confirm the effect of porous structures on the electrochemical performance of CCG electrodes, we conducted EIS measurement at an open circuit voltage with a sinusoidal DC bias of 5 mV in the frequency range of 10 mHz–100 kHz. As typical for supercapacitors, the Nyquist plot of the EIS data consists of three regions [27]: at very high frequency, the supercapacitor behaves like a pure resistor and the equivalent series resistance of the cell can be obtained; at low frequency, the imaginary part sharply increases and a nearly vertical line is observed, indicating a capacitive behavior; in the medium frequency domain, the influence of the electrode porosity can be observed. When the frequency decreases, the signal penetrates deeper and deeper into the porous structure of the electrode and more and more electrode surface becomes approachable for the electrolyte. At a relative lower range, a straight line with 45° occurs. This curve is related to electrolyte diffusion and usually referred to as the Warburg curve [28]. The higher frequency this curve starts, the easier the electrolyte penetrates. From the EIS data of non-porous CCG, macroporous CCG, and CCG with composite pores as shown in Figure 6, we can observe that the starting frequency of the Warburg curve for the non-porous CCG is two orders of magnitude lower than that for the porous CCG. This result confirms that the introduction of pores facilitates the penetration of electrolyte into the inter-layer space of CCG. This is why the porous CCG electrodes showed larger specific capacitance at even relatively high scan rates.

4. Conclusions

Chemically converted graphene with composite pores has been prepared by a photo-catalytic method. The photochemical oxidation of GO mediated by ZnO quantum dots and sp^2 domains of GO led to the formation of both meso/micro-pores (<10 nm) and macropores (>50 nm). Although such graphene still aggregated during hydrothermal reduction and drying, which resulted in a low specific surface area, it exhibited outstanding specific capacitance (up to 350 F g^{-1}), rate performance, and cyclic stability as supercapacitor electrode. The excellent electrochemical properties of the porous graphene are due to (1) the macropores facilitated the penetration of electrolyte into the inter-layer space and (2) the meso/micro-pores increased the adsorption of charges.

Acknowledgements

Jie Tang wishes to thank financial support from the JST ALCA Program and JSPS Grants-in-Aids for Scientific Research 22310074, Japan.

References

[1] A. Burke, J. Power Sources 91 (2000) 37.
[2] J.R. Miller, P. Simon, Science 321 (2008) 651.
[3] A.K. Geim, K.S. Novoselov, Nat. Mater. 6 (2007) 183.
[4] Y.W. Zhu et al., Adv. Mater. 22 (2010) 3906.
[5] M.J. Allen, V.C. Tung, R.B. Kaner, Chem. Rev. 110 (2010) 132.
[6] M.D. Stoller, S.J. Park, Y.W. Zhu, J.H. An, R.S. Ruoff, Nano Lett. 8 (2008) 3498.
[7] J. Xia, F. Chen, J. Li, N. Tao, Nat. Nanotechnol. 4 (2009) 505.
[8] T.A. Yoshida, A. Nishino, J. Electrochem. Soc. 137 (1990) 3052.
[9] Y.W. Zhu et al., Science 332 (2011) 1537.
[10] Z.J. Fan et al., Carbon 50 (2012) 1699.
[11] G.Q. Ning, Z.J. Fan, G. Wang, J. Gao, W.Z. Qian, F. Wei, Chem. Commun. 47 (2011) 5976.
[12] J. Yan, J.P. Liu, Z.J. Fan, T. Wei, L.J. Zhang, Carbon 50 (2012) 2179.
[13] C.G. Liu, Z.N. Yu, D. Neff, A. Zhamu, B.Z. Jang, Nano Lett. 10 (2010) 4863.
[14] R.B. Rakhi, W. Chen, D. Cha, H.N. Alshareef, J. Mater. Chem. 21 (2011) 16197.
[15] Q. Cheng, J. Tang, J. Ma, H. Zhang, N. Shinya, Phys. Chem. Chem. Phys. 13 (2011) 17615.
[16] Y.X. Xu, H. Bai, G.W. Lu, C. Li, G.Q. Shi, J. Am. Chem. Soc. 130 (2008) 5856.
[17] D.Z. Sun, M.H. Wong, L.Y. Sun, Y.T. Li, N. Miyatake, H.T. Sue, J. Sol-Gel Sci. Technol. 43 (2007) 237.
[18] H. Wang et al., J. Solid State Chem. 184 (2011) 881.
[19] Y. Matsumoto et al., J. Phys. Chem. C 115 (2011) 19280.
[20] Y. Zhou, Q.L. Bao, L.A.L. Tang, Y.L. Zhong, K.P. Loh, Chem. Mater. 21 (2009) 2950.
[21] K.P. Loh, Q.L. Bao, P.K. Ang, J.X. Yang, J. Mater. Chem. 20 (2010) 2277.
[22] K.S.W. Sing, D.H. Everett, R.A.W. Haul, R.A. Dierotti, J. Rouquérol, T. Siemieniewska, Pure Appl. Chem. 57 (1985) 603.
[23] E. Frackowiak, V. Khomenko, K. Jurewicz, K. Lota, F. Beguin, J. Power Sources 153 (2006) 413.
[24] V. Khomenko, E. Frackowiak, F. Beguin, Electrochim. Acta 50 (2005) 2499.
[25] Y. Wang et al., J. Phys. Chem. C 113 (2009) 13103.
[26] Y.W. Zhu, S. Murali, M.D. Stoller, A. Velamakanni, R.D. Piner, R.S. Ruoff, Carbon 48 (2010) 2106.
[27] J. Kötz, M. Hahn, R. Gallay, J. Power Sources 154 (2006) 550.
[28] C. Portet, P.L. Taberna, P. Simon, C. Laberty-Robert, Electrochim. Acta 49 (2004) 905.